Title

Nanoengineered shear-thinning and bioprintable hydrogel as a versatile platform for biomedical applications

Authors

Zandi, Nooshin
Sani, Ehsan Shirzaei
Mostafavi, Ebrahim
et al.

Publication Date

2021

DOI

10.1016/j.biomaterials.2020.120476

Peer reviewed

HHS Public Access

Author manuscript

Biomaterials. Author manuscript; available in PMC 2022 January 01.

Published in final edited form as:

Biomaterials. 2021 January ; 267: 120476. doi:10.1016/j.biomaterials.2020.120476.

Nanoengineered Shear-Thinning and Bioprintable Hydrogel as a Versatile Platform for Biomedical Applications

Nooshin Zandi[1,2], **Ehsan Shirzaei Sani**[3], **Ebrahim Mostafavi**[2], **Dina M. Ibrahim**[4], **Bahram Saleh**[2], **Mohammad Ali Shokrgozar**[5], **Elnaz Tamjid**[6], **Paul S. Weiss**[7,8,9,10], **Abdolreza Simchi**[1,11,*], **Nasim Annabi**[3,12,*]

[1]Institute for Nanoscience and Nanotechnology, Sharif University of Technology, P.O. Box 11365-11155, Tehran, Iran

[2]Department of Chemical Engineering, Northeastern University, Boston, Massachuestts 02115, United States

[3]Department of Chemical and Biomolecular Engineering, University of California, Los Angeles, Los Angeles, California 90095, United States

[4]Biotechnology Graduate Program, School of Sciences and Engineering, The American University in Cairo, New Cairo, 11835, Egypt

[5]National Cell Bank Department, Pasteur Institute of Iran, Tehran 13164, Iran

[6]Department of Nanobiotechnology, Faculty of Biological Sciences, Tarbiat Modares University, P.O. Box 14115-175, Tehran, Iran

[7]Department of Chemistry and Biochemistry, University of California, Los Angeles, Los Angeles, California 90095, United States

[8]California NanoSystems Institute, University of California, Los Angeles, Los Angeles, California 90095, United States

[9]Department of Bioengineering, University of California, Los Angeles, Los Angeles, California 90095, United States

[*]Corresponding Authors: Nasim Annabi, Department of Chemical and Biomolecular Engineering, University of California, Los Angeles, Los Angeles, California 90095, USA, nannabi@ucla.edu, Abdolreza Simchi, Department of Materials Science and Engineering, Sharif University of Technology, P.O. Box 11365-11155, Tehran, Iran, simchi@sharif.edu.

CRediT author statement

Nooshin Zandi: Conceptualization, Methodology, Formal analysis, Investigation, Data Curation, Writing - Original Draft, Writing - Review & Editing, Project administration. **Ehsan Shirzaei Sani:** Investigation, Writing - Review & Editing, Formal analysis. **Ebrahim Mostafavi:** Investigation, Writing - Review & Editing, Formal analysis. ***Dina M. Ibrahim*:** Investigation, Formal analysis: **Bahram Saleh**: Investigation: **Mohammad Ali Shokrgozar:** Supervision. **Elnaz Tamjid:** Supervision. **Paul S. Weiss:** Writing - Review & Editing. **Abdolreza Simchi:** Writing - Review & Editing, Supervision, Resources, Funding acquisition. **Nasim Annabi:** Conceptualization, Supervision, Writing - Review & Editing, Resources, Funding acquisition, Validation.

Declaration of interests

The authors declare that they have no known competing financial interests or personal relationships that could have appeared to influence the work reported in this paper.

Supplementary data to this article can be found online at https://doi.org/10.1016/j.biomaterials.2020.120476.

[10]Department of Materials Science and Engineering, University of California, Los Angeles, Los Angeles, California 90095, United States

[11]Department of Materials Science and Engineering, Sharif University of Technology, P.O. Box 11365-11155, Tehran, Iran

[12]Center for Minimally Invasive Therapeutics (C-MIT), California NanoSystems Institute (CNSI), University of California, Los Angeles, 570 Westwood Plaza, Los Angeles, California 90095, United States

Abstract

The development of bioinks based on shear-thinning and self-healing hydrogels has recently attracted significant attention for constructing complex three-dimensional physiological microenvironments. For extrusion-based bioprinting, it is challenging to provide high structural reliability and resolution of printed structures while protecting cells from shear forces during printing. Herein, we present shear-thinning and printable hydrogels based on silicate nanomaterials, laponite (LA), and glycosaminoglycan nanoparticles (GAGNPs) for bioprinting applications. Nanocomposite hydrogels (GLgels) were rapidly formed within seconds due to the interactions between the negatively charged groups of GAGNPs and the edges of LA. The shear-thinning behavior of the hydrogel protected encapsulated cells from aggressive shear stresses during bioprinting. The bioinks could be printed straightforwardly into shape-persistent and free-standing structures with high aspect ratios. Rheological studies demonstrated fast recovery of GLgels over multiple strain cycles. *In vitro* studies confirmed the ability of GLgels to support cell growth, proliferation, and spreading. *In vitro* osteogenic differentiation of pre-osteoblasts murine bone marrow stromal cells encapsulated inside the GLgels was also demonstrated through evaluation of ALP activity and calcium deposition. The engineered shear-thinning hydrogel with osteoinductive characteristics can be used as a new bioink for 3D printing of constructs for bone tissue engineering applications.

Keywords

3D bioprinting; Biomimetic proteoglycan; Osteoinductive bioink; Nanocomposite; Laponite

1 Introduction

Hydrogels, three-dimensional (3D) hydrophilic polymer networks, are extensively used for biomedical applications due to their natural moisture content, biocompatibility, and similarity of their physical and biological properties to native tissues [1–3]. Recently, printable hydrogels have developed for engineering complex cell-laden 3D constructs for tissue engineering applications [4–6]. Shear-thinning hydrogels have many advantages compared to other biomaterials for 3D bioprinting. Their rheological properties, including Herschel-Bulkley flow and stress-relaxation behavior, make them injectable through a needle or catheter [7]. Although the use of shear-thinning hydrogels has recently gained much attention as bioinks, the development of cell-responsive bioinks that can provide high structural reliability and precision has been lacking, to date [8].

Two main approaches, including covalent and non-covalent methods, are used to crosslink hydrogels [9]. Different types of hydrogels have been developed based on covalent crosslinking approaches, which are initiated through the addition of a chemical crosslinker [10], radical polymerization by light exposure [11], or changes in temperature [12] or pH [13]. As crosslinking through covalent bounds forms a permanent network, this method results in construction of robust, tough, and elastic networks. However, most common chemical crosslinkers are toxic and their fate in native tissues and organs are not understood well [14, 15]. As a result, additional purification may be required before their use in biomedical applications. Moreover, covalently crosslinked hydrogels lack self-healing capability, *i.e.*, recovering to initial state when the applied stress is removed. For these crosslinked hydrogels, the arrangement of their networks is disrupted when the material undergoes deformation (*e.g.*, injection forces through a needle or catheter).

Unlike covalently crosslinked hydrogels, most physically crosslinked hydrogels, developed by ionic interactions, complexation, or aggregation approaches, can reform spontaneously [16]. Self-assembly approaches using non-covalent crosslinking, which involve hydrogen bonds, electrostatic, host-guest, and hydrophobic interactions or a combination of them, enable fabrication of moldable, printable, and injectable hydrogels with shear-thinning properties [17]. Self-healing hydrogels with viscous flow under extrusion pressure are attractive materials for 3D bioprinting [4]. Practically, low shear viscosity is advantageous for bioprinting because thinner needles (high gauge) can be used while shielding cells from high shear forces [15]. Such hydrogel systems are utilized for both bioprinting and implantation *in vivo via* direct injection [18]. In addition, approaches based on increased affinity between polymers and hard nanostructure surfaces (*e.g.*, silicate nanoplatelets) have previously been used to fabricate shear-thinning hydrogels [16]. Engineered nanocomposite hydrogels have been widely used for cell delivery [6, 19], growth factor delivery [17], and the development of embolic biomaterials for endovascular embolization [20]. However, cell proliferation and spreading are typically limited by insufficient cell binding sites within these nanocomposite hydrogels or their inappropriate mechanical stiffness, which may hinder their usage as tissue engineering scaffolds [21]. Therefore, it is essential to develop shear-thinning and self-healing bioinks that can effectively support 3D cell growth and proliferation.

The applications of bioprinting have been limited due to the lack of suitable bioinks to meet both 3D printing and tissue engineering demands [22]. Ideal bioinks should not only be capable to form mechanically stable 3D constructs, but also must protect cells through printing process and provide a suitable environment for remodeling into the target tissue [23]. Combining all these requirements to develop bioinks with good printability and biocompatibility to form high resolution 3D structures is challenging [7]. Therefore, intensive studies have been performed to develop printable and structurally stable bioinks which can also preserve encapsulated cells [24]. Recent studies have shown that incorporation of laponite (LA) inside hydrogels can significantly promote the rheological and mechanical properties of resulting biomaterials [21, 25]. Furthermore, *in vitro* studies have also revealed that LA improves chondrogenic differentiation of human bone marrow stromal cells (hBMSCs) and stimulates osteogenic differentiation of human mesenchymal stem cells (hMSCs) without the use of growth factors [17]. On the other hand, the

physiological characteristics of glycosaminoglycans (GAGs) [26] make these polymers promising candidates to prepare hydrogels through hybridization with silicate nanomaterials. Glycosaminoglycans in native tissue are covalently bound to proteins, forming the basic proteoglycan. Once bound to proteins, GAGs react with several superficial cell sites [27]. Naturally and chemically modified GAGs have been shown to induce osteogenic differentiation of hMSCs [28, 29]. However, to our knowledge, there has been no report of engineering shear-thinning hydrogels based on glycosaminoglycan nanoparticles (GAGNPs).

In this study, we report the formation of a hydrogel-based bioink (GLgel) that combines GAGNPs with LA as a versatile strategy to generate cell-laden bioprinted constructs. We investigate the effects of GAGNPs on the printability, and rheological properties, swelling and degradation characteristics of the nanoengineered GAGNPs/LA hydrogels. We then evaluate the *in vitro* biocompatibility and osteogenic properties of the resulting hydrogels. Finally, the engineered shear-thinning hydrogels are used as bioinks for printing cell-laden constructs with freestanding and high shape fidelity. These shear-thinning hydrogels can be used as osteoinductive bioinks for printing cell-laden complex constructs.

2 Materials and Methods

Materials

Chondroitin sulfate B sodium salt (from porcine intestinal mucosa, ≥90%, lyophilized powder, 60 kDa; PDI = 1.94) and poly-L-lysine (PLL) (0.1 % w/v in H_2O), sodium acetate, sodium chloride, potassium chloride, sodium phosphate dibasic, paraformaldehyde, Triton, bovine serum albumin (BSA), and potassium phosphate monobasic were obtained from Sigma-Aldrich (St. Louis, MO, USA). 2D clay particles (Laponite XLG) with a thickness of 1 nm and lateral dimensions of 20 − 50 nm were obtained from BYK Additives Inc (Rochester Hills, MI, USA). Dulbecco's phosphate-buffered saline DPBS (Gibco), Dulbecco's modified eagle medium (DMEM) media (Gibco), Minimum Essential Medium Alpha (MEM α), ethidium homodimer-1 (EthD-1), Calcein AM, PrestoBlue assay, Alexa Fluor 594−phalloidin, and 4′,6- diamidino-2-phenylindole (DAPI), and rhodamine-phalloidin were purchased from Thermo Fisher Scientific (USA). QuantiChrom Calcium Assay kit, and QuantiChrom Alkaline Phosphatase Activity kit were purchased from BioAssay Systems (Hayward, CA, USA).

Preparation of Proteoglycan Nanoparticles (GAGNPs)

To form GAGNPs, chondroitin sulfate sodium salt (1.8 mg mL^{-1}) (polyanion) and PLL (1 mg mL^{-1}) (polycation) were each dissolved in 0.1 M acetate buffer (pH = 5.5) under vigorous mixing [30]. The solutions were then filtered by using a poly(vinylidene fluoride) syringe filter (0.22 μm, Thermo Fisher Scientific) to remove aggregated particles. The PLL solution was then added dropwise to an excess amount of GAG (1:6 volumetric ratios) under vigorous stirring. The resulting mixtures were settled overnight, and the supernatant solution was then decanted and centrifuged at 6000 RCF for 15 min. Finally, the precipitates were lyophilized (Labconco, USA) to obtain GAGNPs as a white powder.

Preparation of shear-thinning nanocomposite bioinks (Glgels)

Dispersed LA was prepared by exfoliating LA powder in miliQ water followed by vortexing for 20 min. GAGNPs solution was then quickly mixed with the LA dispersion and immediately vortexed for 1 min to yield homogenized gels. Different concentrations of LA (20, 25, 30, and 35 mg mL^{-1}) at fixed GAGNPs/LA weight ratio (1:120) were used to prepare different GLgel compositions (20GLgel, 25GLgel, 30GLgel, and 35GLgel). Final concentrations of GAGNP in 20, 25, 30, and 35GLgels were 0.17, 0.21, 0.25, and 0.3 mg mL^{-1}, respectively. All GLgels solutions were used immediately for rheological analysis.

Scanning electron microscopy (SEM)

SEM images of GLgel were taken using a Hitachi S-4800 SEM at an acceleration voltage of 3 kV. After preparing the hydrogel, 1 ml glucose solution (0.1 M) was added to 0.5 ml of the gel in order to preserve the gel structure during freeze drying. The gel was then flash frozen in liquid nitrogen followed by lyophilization (Labconco, USA). Finally, the lyophilized gel was placed on aluminum stubs and sputter coated by gold/palladium (about 6 nm) before imaging.

Transmission electron microscopy (TEM)

TEM images of GAGNPs where acquired using a JEM-1010 (JEOL, Tokyo, Japan) machine. To prepare the samples, a drop of the diluted suspension of GAGNPs was placed on a copper-coated grid (Formvar/Carbon 200 mesh, Copper) and air dried prior to imaging.

In vitro swelling

GLgels were flash frozen in liquid nitrogen and lyophilized overnight. The original weights of the samples were then measured, and each sample was placed in a Transwell insert with 1 μm pores. Next, 1 mL of DPBS was added to the wells and another 300 μL of DPBS was added to the Transwell inserts to prevent the surface of the GLgels from drying during incubation. The well plates were then incubated at 37 °C for 24 h. At each selected time point, the weights of swollen samples were measured. The swelling ratio (SR%) was calculated using the following equation [31]:

$$SR(\%) = \frac{W_{wet} - W_{dry}}{W_{dry}} \times 100 \quad (2)$$

where W_{dry} represents the weight of initial dry and W_{wet} is the weight of the wet samples after swelling at different time points.

In vitro degradation

Samples were weighed and transferred to 1.5 mL microcentrifuge tubes containing 500 μL DPBS and incubated at 37 °C for different time points (up to 28 days). At each time point, the samples were removed from solution, lyophilized overnight, and re-weighed. The weight loss (WL%) was determined according to equation 3 [32]:

$$WL(\%) = \frac{W_i - W_f}{W_i} \times 100 \quad (3)$$

where W_i represents the initial weight and W_f is the weight of the samples after swelling at time t.

Zeta potential analysis

Zeta potentials of the particles were determined by a Malvern Zetasizer (Ver. 6.00, UK). To do this, a suspension of LA (10 mg mL^{-1}) was prepared and mixed with GAGNP suspensions with different concentrations in the range of 0.025 to 0.25 mg mL^{-1}. In addition, LA (10 mg mL^{-1}) and GAGNPs (0.025–0.25 mg mL^{-1}) suspensions were separately analyzed as controls.

Evaluation of compressibility and injectability

The injectability of GLgels was evaluated using an Instron mechanical tester (Instron 5542). Briefly, the materials were placed in 3 mL plastic syringes and then fixed between upper compression platen and lower tensile grips. The gels were then injected through a medical catheter (5-French Beacon). The injection rate was controlled by changing the cross speed of the compression platen to achieve the desired flow rates. The amount of force (N) to inject the material was then determined using a Bluehill version 3 software ($n \geq 3$).

To determine the mechanical characteristic of GLgels, compression test was performed on cylindrical specimens (6 mm in diameter and 1.8 mm in height) prepared by injection of the gels inside polydimethylsiloxane (PDMS) molds. The gels were transferred to 3 mL syringes and the trapped bubbles were removed by centrifugation (2000 rpm for 2 min). After injection of ~1 mL gel solution per mold, the solidified samples were removed from the molds. Compression tests were performed at a strain rate of 1 mm min^{-1}. Compression moduli were calculated from the slopes of loading stress vs strain curves at strain levels between 0–10%, as described previously ($n \geq 3$) [33].

Rheological tests

A hybrid rheometer (Discovery HR-1) was used to investigate the viscoelastic properties of the LA and GLgel samples. A parallel-plate geometry (40 mm diameter) with 27 μm gap distance was used for rheological assessments. Angular frequency sweep was evaluated to measure storage (G′) and loss (G″) moduli with frequencies from 0.1 to 100 rad s^{-1} in a linear strain region of 0.1%. Additionally, the steady shear rate sweep (10^{-3} to 10 s^{-1}) was measured to characterize the behavior of the materials. Shear recovery experiments were performed at the stepwise strain of 100% with 0.1% strain recovery at 1 Hz frequency (5 min for each step). Strain sweeps were performed across a strain range of 0.001% to 100% at 1 rad s^{-1} frequency. Steady shear properties were measured over a range of 10^{-3} to 10^2 s^{-1}. To evaluate the shear recovery of the samples, step strain was measured at a high strain (100%) with recovery at a low strain (0.1%). G′ and G″ modules were recorded for three cycles at the frequency of 1 Hz. All rheological examinations were repeated at least three times ($n \geq 3$).

2D cell encapsulation

NIH 3T3 cells (American Type Culture Collection (ATCC) (Manassas, VA, USA) were cultured at 37 °C and 5% CO_2 in Dulbecco's modified eagle medium (DMEM) supplemented with penicillin/streptomycin (1% (v/v)) and FBS (10% (v/v)). 30GLgel and 35GLgel were selected for 2D cell culturing. 2D cell seeding was performed as described elsewhere [34]. Briefly, 10 μL of the gels were pipetted on the surface of a glass slide and spread over it to cover 1 × 1 cm area. After placing the samples in 24 well-plate, 3T3 cells were seeded on the hydrogel surface (10^5 cells gel^{-1}) and incubated in humidity 95% containing 5% CO_2 for 45 min at 37 °C. Next, 400 μL of media was added to each well, and incubated for 7 days. The culture media was replaced with fresh media every day.

3D cell encapsulation

W-20–17 stromal cells were cultured in Minimum Essential Medium Alpha (MEMα) supplemented with 10% (v/v) FBS and 1% (v/v) penicillin/streptomycin at 37 °C and 5% CO_2. Prior to cell encapsulation, the GLgels were sterilized through UV exposure for 30 min. For 3D cell encapsulation, 30GLgel precursor solution was prepared in DPBS and mixed gently with the cells (10^7 cells mL^{-1}). A 10 μL of the mixture was then pipetted on a spacer with a thickness of 150 μm and then covered by a glass slide. The cell-laden gel was then placed in a 24 well plate and incubated at 37 °C for 5 days.

Cell viability and metabolic activity

A commercial Live/Dead assay kit (Invitrogen) was utilized to determine the viability of cells after 1, 3, and 5 days following 2D and 3D cultures. Briefly, cells were stained with ethidium homodimer-1 (EthD-1, 2 μL mL^{-1} in DPBS) for dead cells and Calcein AM (0.5 μL mL^{-1} in DPBS) for live cells. The samples were then incubated for 15 min at 37 °C and then washed three times with DPBS to remove the remaining stains. Finally, stained samples were imaged using an inverted fluorescence microscope (Zeiss Axio Observer Z1, Carl Zeiss microscopy). The obtained images were analyzed using ImageJ software (National Institutes of Health, USA) to calculate cell viability (%) by dividing the number of live cells by the total cell number [35]. Metabolic activity of the cells was assessed using a PrestoBlue assay (Thermo Fisher Scientific) according to the manufacturer's instructions. Briefly, cell seeded hydrogels were incubated in 500 μL of growth media. After 1, 3, and 5 days of culture, 10% of the media was removed and replaced with an equal amount (50 μL) of PrestoBlue solution. Next, the cells were incubated for 45 min at 37 °C/5% CO_2. Fluorescence intensity of the solutions was recorded using a plate reader (Synergy HT fluorescence, BioTek) at 535–560 nm excitation and 590–615 nm emission [36].

Cell adhesion, spreading and proliferation

Cell adhesion and spreading were evaluated through fluorescent staining of F-actin filaments with Alexa Fluor 594−phalloidin (Invitrogen) and cell nuclei with DAPI. Briefly, the cells were fixed in 4% (v/v) paraformaldehyde (Sigma) for 20 min and then permeabilized with 0.1% (w/v) Triton X-100 solution in DPBS for 45 min. Next, 1% (w/v) bovine serum albumin (BSA) solution in DPBS was used to block the samples for 20 min. Samples were then incubated with Alexa-fluor 488 phalloidin (1:400 dilution in 0.1% BSA, Invitrogen) at

37 °C for 45 min. After three times washing with DPBS, the samples were counterstained with 1 μL/mL DAPI in DPBS for 5 min followed by three times consecutive washing with DPBS. Fluorescent images were acquired using an inverted Axio Observer Z1 microscope. The number of cell nuclei stained with DAPI was counted by using ImageJ software [11].

Calcium deposition assay

Calcium deposition tests were performed using a QuantiChrom Calcium Assay kit according to the manufacturer's protocol. Briefly, cells (10^5 cell mL^{-1} gel) were seeded on 30GLgel, 30LA and polystyrene tissue culture well-plate as control. The samples were then incubated at 37 °C and 5% CO_2 for 7 days. At different time points (1, 5, and 7 days), the samples were washed with DI water, followed by adding 0.60 M HCl (1 ml) and incubating at room temperature for 4 h on a shaker (120 rpm). Cell lysates were centrifuged at 12,000 rpm for 3 min, and 5 μL of the supernatant of each sample was mixed with 200 μL of the working reagent and incubated at room temperature for 3 min. Absorbance intensity was recorded at 612 nm by using a plate reader (Bio-Tek Inc). Calcium concentrations were determined from a standard calibration curve[37].

Quantification of calcium and Phosphorus

Mineral formation in cell-seeded scaffolds (30GLgel and 30 LA) and TCP was measured by coupled plasma mass spectrometry (ICP-MS) after 7 days of incubation. Calcium and phosphorus were detected in both scaffolds and TCP. The samples were transferred to a digestion tube, then digested with concentrated nitric acid (67–70%). This solution was then introduced to ICP-MS (NexION™ 350D ICP-MS, PerkinElmer, USA) for the elemental analysis.

Alkaline phosphatase activity assay

Alkaline phosphatase (ALP) activity was measured using a QuantiChrom Alkaline Phosphatase Activity assay according to the manufacturer's protocol. Briefly, cells (10^5 per 1 mL gel) were seeded on 30GLgel, 30LA and tissue culture well plates. After washing with PBS, samples were incubated with 0.2% Triton for 20 min at room temperature on a shaker (120 rpm). Next, 2 μL of pNPP, 200 μL of assay buffer, and 5 μL of Mg acetate solutions were added to 50 μL of the cell lysates. The same amount of the reagents was added to 50 μL mili-Q water as a blank control. The absorbance was read at 405 nm immediately and after 4 min and the ALP content was calculated according to equation (4):

$$\text{ALP content} = \frac{(OD_{sample(t)} - OD_{sample(0)}) \times Vol_{reaction}}{(OD_{calibrator} - OD_{water}) \times Vol_{sample(t)}} \times 35.3 \quad (4)$$

where $OD_{Sample(t)}$ and $OD_{Sample(0)}$ are OD_{405nm} values at t = 4 min and t = 0, respectively.

3D Bioprinting

30GLgel was used as a bioink for bioprinting purposes. The bioink was loaded into a 3 mL syringe and centrifuged at 2000–3000 rpm for 1 min to remove the trapped bubbles. Food coloring was used to increase the visibility of the bioink. All the 3D printing was performed using an Inkredible+ 3D bioprinter (Cellink, USA) at room temperature, with a moving

speed of 100%, filament gaps of 1 mm, and nozzle gauge of 25G. During the process, the extrusion pressure was changed from 50 to 85 kPa to optimize the bioprinting conditions. A 3D CAD drawing software was used to generate stereolithography (STL) files and converted to G-codes using Slic3r toolbox. Rectangle structures (2 cm × 2 cm) were built by replicate printing of multilayers with height of 1 mm. Hollow cylinders were also printed with an outer diameter of 1 cm, inner diameter of 0.9 cm, and height of 2 cm.

To print cell-laden constructs, W-20–17 stromal cells (5×10^6 cell mL^{-1}) were mixed with GAGNP suspensions, and LA solution was added to form homogenies 30GLgel. The cell-laden bioink was then transferred into a 3 mL syringe and printed on the glass slides to form cubic and cylindrical constructs. The bioprinted samples were then kept in 12-well plates containing cell culture media and incubated at 37 °C. PrestoBlue assay was performed on days 1, 5, and 7 post culture to quantify the metabolic activity of the cells in the bioprinted constructs. F-actin staining was performed to investigate the adhesion and spreading of the cells within the bioprinted constructs after 1 and 5 days. The stained cells were visualized by using an Axio Observer Z1 fluorescent microscope (Carl Zeiss microscopy).

In vivo biocompatibility and biodegradation of GLgel

For the *in vivo* studies, adult male Wistar albino rats (200–250 g) were used in compliance with a protocol approved by the research ethics committee of College of Science, University of Tehran. Under isoflurane anesthesia, 100 μL of 30GLgel was injected in the back of the rats using a 31G needle. The animals were sacrificed at day 7 and day 14 post-injection. The subcutaneous tissues were harvested at the injection site. Tissues were fixed in 10% formalin for 15 min and then embedded in paraffin block. Cross sections were stained with hematoxylin and eosin (H & E). Images were obtained for each specimen by an inverted microscope Eclipse Ti (Nikon, Melville, NY).

Statistical Analyses

Results were reported as mean ± standard deviation (SD). One-way and two-way analysis of variance (ANOVA) was carried used for data analysis using a GraphPad Prism 7.0 software. Significance levels were presented as *$p < 0.05$, **$p < 0.01$, ***$p < 0.001$, and ****$p < 0.0001$.

3 Results and Discussion

GLgel synthesis

Reversible interactions between LA and GAGNPs formed a nanocomposite hydrogel network, named GLgel, through self-assembly, which enabled complete recovery of structural integrity while supporting encapsulated cells (Scheme 1). The LA nanoparticles have negatively charged surfaces (*ca.* 1000 negative charges per particle) with positively charged edges (approximately 10% of the total charge) [2]. The porous structure of GLgel was formed as a combination of oppositely charged nanostructures (positively charged LA edges and negatively charged GAGNPs). In addition, the high surface areas of both LA and GAGNPs provided sufficiently dynamic interactions to form the hydrogel network. Using this technique, we engineered different compositions of GLgels including 20Glgel, 25Glgel,

30Glgel, and 35Glgel based on various concentrations of LA and GAGNPs, as summarized in Table 1.

Recently, the interactions between different polymers such as poly (ethylene glycol) (PEG) and Laponite has extensively investigated [38–40]. Also, there are several studies which report development of bioink containing LA and different polymer such as heparin [41], (PEG) [7], gelatin methacryloyl (GelMA) and kappa-carrageenan (κCA) [7]. However, engineering shear-thinning bioinks based on LA and polymeric nanoparticles has not been studied. Therefore, we aimed to develop new bioinks containing polymeric nanoparticles and LA for injection and bioprinting applications.

The gel forming in LA depends on the electrostatic interactions through face-to-edge of these nanoparticles [2]. The electrostatic interactions between GAGNPs and LA could provide crosslinks which may resulted in gel formation (Figure 1A). Therefore, we used zeta potential to evaluate the change of charges after mixing these two components. To this end, the LA concentration was 10 mg/mL, so that it could interact with GAGNPs to form complex without gelation. Higher concentration can prevent the mobility of conductive particles for evaluation of zeta potential. The concentration of GAGNPs in the GL complex suspensions was in the range of 0.02 to 0.22 mg/mL. Compare to the zeta potential of GAGNPs and LA as control, the GL complexes showed little decrease in zeta potential at GAGNPs:LA ratio between 1:500 and 1:250. This was followed by a relatively higher drop between 1:250 and 1:80 mg/mL and then reached a plateau between 1:80 and 1:53. The zeta potential profile for GAGNPs:LA ratio in the range of 1:250 to 1:80 showed that most of the negatively charged GAGNPs were bound to the positively charged LA edges. Few free GAGNPs contributed to the zeta potential at this range. The drop in the zeta potential between 1:250 and 1:80 mg/mL of GAGNPs:LA ratio could be due to a saturating absorption of GAGNPs to LA. Above this threshold, free GAGNPs mainly contributed to zeta potential value in a similar manner to the control GAGNPs solution (Figure 1A). Taken together, the zeta potential measurement offered evidence for the for electrostatic interactions between GAGNPs and LA edges.

Additionally, the hydrodynamic diameter of LA, GAGNPs and GL mixtures were measured using DLS. To measure the nanoparticles diameter, each solution was diluted at a fixed GAGNPs:LA ratio (1:120). The results showed that the mean size diameters were 4.1±0.2 nm and 171±30 nm for LA and GAGNPs, respectively. Upon mixing the nanoparticle solutions, the mean diameter size reached 7.3±1.5 due to the higher concentration of LA as compared to GAGNPs in the GL complex where colloidal aggregation was not formed (Table S1).

In contrast to common preparation methods that require repeated heating/cooling cycles [42], ultrasonication [43], *in situ* polymerization [44], crosslinking reactions [45], or a combination of them, GLgel is formed easily by mixing two components in water at ambient temperature. Reversible interactions between LA and GAGNPs govern hydrogel formation through self-assembly with shape-persistent properties. Interestingly, complete recovery of structural integrity after removing shear stresses was attained. Scanning electron microscopy (SEM) images of lyophilized GLgel (*e.g.*, 30GLgel) exhibited a highly interconnected

porous network (Figure 1B). GAGNPs are composed of glycosaminoglycan and poly-L-lysine (PLL), which mimic proteoglycan structures in native ECM. Transmission electron microscopy (TEM) images of GAGNPs indicated individual spherical particles with an average diameter of 60 ± 11 nm (Figure 1C,D). The hydrogel also exhibited appropriate structural stability after 3 weeks incubation in Dulbecco's phosphate-buffered saline (DPBS) at 37 °C (Figure S1A).

Injectability and mechanical strength of GLgel

As the injectability of the developed GLgel is critical for bioprinting, the required force to inject the hydrogel through a clinical 5-French catheter (ID = 0.97 mm), at a fixed flow rate of 34 cm min^{-1}, was measured using an Instron mechanical tester (Figure 2A). The injection force increased linearly with time and then plateaued, showing stable, steady flow. The plateau profile indicated that the hydrogel began to extrude through the catheter (Figure S1B). The injection force values of LA samples were 1.4 ± 0.1, 4.0 ± 0.2, 8.0 ± 0.5, and 9.6 ± 0.4 for 20LA, 25LA, 30LA, and 35LA, respectively (Figure 2B). However, upon mixing GAGNPs with LA for all compositions, the injection force increased significantly, as compared to pure LA. The injection force was increased from 6.43 ± 0.40 for 20GLgel to 10.5 ± 0.5, 16.6 ± 0.6, 17 ± 0.2 for 25GLgel, 30GLgel, and 35GLgel, respectively (Figure 2B). These results indicated strong interactions between the two components, depending on the compositions of GLgel. For all compositions, the hydrogels flowed easily from the catheter at relatively low pressure and could be injected by hand.

The Young's moduli of GLgels were measured to quantify the mechanical stiffness of printable hydrogels (Figure 2C and S1C). As made, LA dispersions up to 35 mg mL^{-1} concentration (35LA) were unable to form stable gel through face-to-edge interactions; therefore, measurement of the compression modulus of resulting weak networks was not possible. However, when combined with even low concentrations of GAGNPs (<0.3 mg mL^{-1}), stable hydrogel networks were formed (Figure 2D). This result suggests that without the use of any crosslinking agents, GLgels with tunable compressive modulus could form with varying concentrations of GAGNPs and LA. The compressive modulus was increased from 0.7 ± 0.1 kPa for 20GLgel to 2.4 ± 0.3, and 4.6 ± 0.2 kPa, for 25GLgel, 30GLgel, respectively. However, the modulus decreased to 3.1 ± 0.1 kPa for 35GLgel. This decrease could be due to the lack of sufficient interactions between GAGNPs and LA at this concentration.

In Vitro swelling ratio and degradation properties of GLgel

Swellability of hydrogels and their stability in physiological environment are important parameters as they determine their high permeability and stability during the tissue regeneration process [46, 47]. We studied the effect of GLgel compositions (with 20, 25, 30, and 35GLgel) on the swelling ratio and *in vitro* degradation of the hydrogels. For comparison, hydrogels based on LA suspensions (20, 25, 30, and 35LA) were examined as controls. LA platelets enable formation of weak gels through "house-of-card" structures, which are time and concentration dependent [48]. Since LA suspensions (up to 35 mg mL^{-1}) could not form hydrogel networks rapidly through house-of-card structures, the experiment was conducted after 48 h incubation of LA solutions at room temperature to ensure

formation of weak hydrogel networks based on LA. As shown in Figure 2E,F, the values for swelling ratios varied with both incubation time and hydrogel composition. Generally, for both LA and GLgels, the highest swelling ratio was observed after 6 h. In addition, the networks formed based on LA showed drops in swelling ratios from 16 to 24 h, which could be due instability of the LA gels. The swelling ratios of GLgels after 24 h reached to 3,039 ± 80% for 20GLgel, 2,324 ± 90% for 25GLgel, 4,795 ± 100% for 30GLgel, and 1,834 ± 200%for 35GLgel. In contrast to LA (Figure 2F), no weight loss was observed for GLgels, which we attribute to their improved structural stability in physiological conditions and sustained integrity. In addition, the swelling ratio of GLgels was tunable with different hydrogel compositions.

The degradation of hydrogels in DPBS at 37 °C was evaluated at different time points by measuring the dried weight loss (Figure 2G–H). Complete degradation for all formulations of LA gels was observed after 14 days incubation in DPBS at 37 °C. However, the GLgel group lost only up to 23% of their masses over the same period of time. GLgels continued to be stable up to 21 days incubation in DPBS. Under this condition, the materials retained up to 60% of their initial mass after 28 days of incubation. We attribute the stability of the GLgel in DPBS to the interactions between LA and GAGNPs in the hydrogel network.

Viscoelastic properties of GLgel

Rheological properties of the engineered GLgels including angular frequency, shear rate sweep, and strain sweep analysis were examined at 25 °C (Figure 3). Angular frequency sweep profiles indicated that all compositions of GLgels had stable G' values which were ~20 times greater than G'' in the range of 0.1 to 100 rad s^{-1}. These results confirmed the zeta potential data, indicating that GAGNPs and LA were able to form stable networks quickly at a certain GAGNPs:LA ratio (1:120), which was used in all GLgels (Figure 3A). In the case of GLgel, the two components rapidly formed network structure, and some of the anchored GAGNPs were shared by the adjacent LA to form crosslinks. Therefore, 1:120 GAGNPs:LA was suitable to form stable gel. Regarding zeta potential analysis, a higher GAGNPs:LA ratio (1:80) was required for the saturating absorption. Shear rate sweep measurements demonstrated that all compositions of GLgel exhibited shear-thinning behavior in which the viscosity of material depended on the shear force required for hydrogel extrusion. In contrast, shear rate sweep measurements of LA (30LA) as a control indicated that the viscosity did not change with shear rate, as derived from Newtonian fluid properties (Figure 3B). As shown in Figure 3B (inset), a homogeneous gel was formed upon injection through a syringe. Previous studies on the injectability of gels containing oppositely charged dextran microspheres showed filter-pressing effect [49]. This filter-pressing phenomenon was not observed in our nanoscale-based system due to the smaller pore sizes in the GLgel network, which decreased the aqueous phase flowability [50]. The injectability of the material is related to its ability to remain homogeneous under pressure without phase separation [51].

The relationship between viscosity (η) and shear rate (γ) can be expressed by the following power-law equation [18]:

$$\eta = K \cdot \gamma^{(n-1)}$$

where K and n describe the consistency index and flow index, respectively. The latter (n) is a critical parameter to characterize the flow properties of a material, where $n < 1$ indicates shear thinning, $n > 1$ shear thickening, and $n = 1$ represents Newtonian flow. According to the power law, the derived "n" values were calculated to be 0.12 ± 0.06, 0.18 ± 0.08, 0.26 ± 0.05, and 0.22 ± 0.12 for 20, 25, 30 and 35GLgel, respectively. This observation confirms that small amounts of GAGNPs have a strong effect on LA shear-thinning and viscoelastic properties (Figure 3C). The results also indicated that the presence of GAGNPs increases the shear-thinning behavior of GLgels. This change improves the printability of the GLgels by reducing flow resistance under higher shear rates during the extrusion. The consistency index (K) also increased consistently for 20, 25, and 30GLgel, showing higher viscosities at a constant shear rate. This observation suggests improved packing of LA sheets or "house-of-cards" arrangements at higher LA concentrations, demonstrating increases in viscosity at all shear rates. Importantly, these hydrogels could be injected into aqueous environments while preserving their integrity without the need for stabilizing reactions.

Strain-dependent oscillatory measurements of GLgels displayed consistent linear viscoelastic behavior followed by network failure at high strains (Figures 3D and S2A). At low strains, both storage and loss moduli were independent on strain. Herein, G′ was at least one order of magnitude greater than G″. At a critical strain where G″ ≈ G′, the gel structure was transformed from solid to liquid, showing yielding behavior. In high strain regions, the loss modulus (G″) was increased, and exceeded the storage modulus (G′), indicating liquid-like properties of the GLgels (Figures 3D). The G′ values decreased beyond the critical strain (γ = 9.0%), demonstrating conversion of the hydrogel network from a gel state to a quasi-liquid state (Figure S2A).

By increasing the LA concentration from 20 to 30 mg mL^{-1} in GLgel formulation, the storage moduli and the viscosity enhanced with a similar trend, while 35GLgel did not show a significant increase as compared to 30GLgel (Figure S2A). This difference could be due to the lack of sufficient space between LA layers at 35GLgel, which may prevent GAGNPs from interacting with LA, resulting a less stiff gel. Based on these results, the highest viscosity and storage moduli were obtained for 30GLgel (Figures S2B).

Step-strain experiments were conducted to determine the self-healing behavior of GLgels (Figures 3E and S2C). When the strain was switched between 1% and 100%, the materials displayed an inversion of G′ and G″ at the high strain and quickly recovered their elastic properties at the low strain. Cyclic strain tests (three cycles) with 5 min intervals were also applied to monitor the self-healing efficiency (Figure 3E,F). The results revealed ~99% recovery. Moreover, the recovery of GLgel, in each cycle of breaking and reforming, confirmed the reversible and robust nature of the non-covalently crosslinked GLgel network (Figure 3F). These results suggest that nanoscale-based gels can be pressed more densely than microscale-based materials. Basically, high specific surface area of nanoscale-based hydrogel induces higher resistance to shear forces. Compared to other physically crosslinked gels such as peptide-based hydrogels [52], Glgel recovery was faster. This self-healing

behavior can be attributed to the fast and reversible re-establishment of the electrostatic interactions between oppositely charged GAGNPs and LA. According to the step-strain curves, all gels showed liquid behavior (gel-sol transition, tan delta: $G''/G' > 1$) at high strain (100% strain). At low strain (same frequency (1.0 Hz), G'' values were completely recovered, and the system could return to its previous quasi-solid form (tan delta: <1) (Figure 3G). This observation confirmed the self-supportive and elastic nature of the GLgels, as a result of the strong dynamic interactions and hydrogen bonding between the two components [53].

The shear-thinning properties and rapid recovery of the GLgels make them suitable for extrusion-based bioprinting [54]. Moreover, the dynamic interactions between the components of GLgels enable complete recovery of the viscoelastic properties even after multiple high strain cycles. This recovery is particularly critical for bioprinting applications, as the bioinks can be extruded through multiple layer-by-layer injections without requiring continuous extrusion. We attribute the fast gelation and stable structures of the GLgels to one or more of the following factors: (i) GAGNPs with negative surface charge may diffuse between LA platelets without microscopic aggregation to form network structures; (ii) electrostatic interactions between the two components can rapidly rearrange ionic crosslinking; and (iii) nanometer-size components facilitate uniform gelation due to high surface area, even at low concentrations of GAGNPs.

Since 30GLgel showed the highest compression modulus and suitable rheological properties, this gel composition was used as the bioink for the 3D printing of free-standing and self-supporting structures.

In vitro cytocompatibility of GLgel

NIH-3T3 fibroblast and W-20–17 bone marrow stromal cells were used as model cells to evaluate cell viability, proliferation, and metabolic activity on the 30GLgel. The viability and metabolic activity of the 3T3 cells seeded on the surface of the gels (2D cell seeding) were evaluated by using a commercial Live/Dead (Figure S3A–B) assay and a PrestoBlue kit (Figure S3C), respectively [55]. The results shown high viability (>85%) for the cells seeded on GLgels over 7 days of culture (Figure S3A–B). In addition, the metabolic activity of the 3T3 cells seeded on 30GLgels consistently increased for up to 7 days of culture (Figure S3C), confirming the *in vitro* cytocompatibility of the GLgels.

Previous studies have shown that 2D silicate nanomaterials incorporated in biomaterials promoted cell adhesion and proliferation as they provide suitable cell binding sites while facilitating protein adsorption [18, 48, 56]. Despite numerous studies on the physiological stability and injectability of shear-thinning nanocomposite hydrogels [50, 57, 58], the *in vitro* 3D cell encapsulation within these gels has not been investigated extensively. Therefore, we aimed to evaluate the *in vitro* cytocompatibility of the engineered 30GLgel through 3D encapsulation of W-20–17 stromal cells within the hydrogel network. Live/dead assay, F-actin/ DAPI staining, and PrestoBlue assay were employed to determine the cell viability (Figures 4A–B), cell spreading (Figures 4C), and metabolic activity (Figure 4D), respectively. Cell viability was >95% over 5 days of culture based on the Live/Dead assay (Figure 4B). Accordingly, F-actin staining revealed higher spreading of 3D encapsulated

cells at day 5, when compared to day 1 post encapsulation (Figure 4Ci–ii). Moreover, the metabolic activity of the encapsulated cells was increased during 5 days of culture, showing high cell viability and proliferation (Figure 4D). Taken together, these *in vitro* assessments revealed that the engineered GLgels were cytocompatible and could improve proliferation and spreading of the cells encapsulated within their 3D structures. In contrast to the majority of the previously reported hydrogels [59–61], the GLgel synthesis process did not generate free radicals, which potentially makes it suitable for cell encapsulation purposes.

In vitro osteoinductivity of GLgel

Previous studies have shown that clay minerals not only enhance cellular adhesion and protein adsorption, but also facilitate mineralization and osteogenesis [21, 29]. It has been reported that GAGs also interact with different ligands to regulate cell signaling, migration, and differentiation [62]. Here, we studied the early osteogenic responses of cell-seeded 30LA and the 30GLgel by measuring alkaline phosphatase activity (ALP) and calcium deposition values on days 1, 3, and 7 (Figure 4C,D). To perform these tests, W-20–17 cells were seeded on 30GLgel, 30LA and tissue culture polystyrene (TCPS) plates as control. After 7 days, the cells seeded on 30GLgel exhibited 1.6-fold and 4.5-fold increases in ALP activity, compared to cells seeded on 30LA and TCPS, respectively (Figure 4G). We attribute this improvement to the synergic effects of LA and GAGs on the osteoinductivity of the 30GLgel.

Moreover, the generation of bone-like inorganics in LA and 30 GLgel was confirmed via calcium deposition assay (Figure 4H). The quantification of calcium deposition results showed significant increases in the amount of calcium ions generated on 30GLgel as compared to TCPS (6-fold on day 7). The calcium deposition on 30GLgels was 1.5-fold higher than 30LA on day 7 post-culture (Figure 4H). Furthermore, the bone mineral concentration (Ca and P) was measured using ICP-MS. As shown in Table S2, the total amounts of calcium and phosphorous were greater in the 30GLgel and 30 LA as compared to the TCP. Overall, these results demonstrated the capability of GLgels in promoting osteogenic differentiation of pre-osteoclasts without requiring any supplemental osteoinductive factors.

3D Printing of Hydrogels

The shear-thinning behavior of the GLgels make them suitable for printing precisely designed constructs through direct-write printing (supplementary movie 2). This compatibility is mainly due to the fast recovery of the material to a quasi-solid state with high storage modulus and yield stress. Herein, we investigated the effect of pressure on the printability of the developed bioinks in continuous forms and without any “dash” or “over-flowing” printed shapes. In this case, the pressure was altered from 50 to 85 Pa, while other parameters including temperature (25 °C), nozzle size (25G), and printing speed (12 mm s^{-1}) were kept constant. Printing speed is another essential parameter, especially for fabricating large cell-laden constructs [7]. However, tradeoffs between printing speed and resolution should be considered. Generally, lower printing speeds are required to fabricate high-resolution constructs [63]. However, the high printability of GLgels make it appropriate for high-speed printing of high-resolution constructs. As shown in Figure 5A, the suitable

pressure for printing of the bioink was in the range of 70–80 Pa. In the next step, we printed two different structures to evaluate the printability of the GLgels (Figure 5Bi–ii). First, a lattice construct consisting of individual filaments was printed (Figure 5Biii–iv). Although, conventional bioinks can be used for precise printing in the x and y (lateral) directions, the printing multilayer 3D structures remains challenging. To assess the printability of GLgels on the z-axis, we printed a multilayered hollow cylinder, in the shape of a human-scale blood vessel (9 mm interior diameter and 1 mm thickness). Using 30GLgels, we were able to print a highly stable and self-supported, multi-layer cylinder (25 layers), without using any supporting material (Figure 5Biii,v,vi).

While a variety of bioinks has been used for printing applications, the development of low-concentration bioinks for direct writing without any molding or subsequent chemical crosslinking is challenging. In contrast, the electrostatic interactions between LA and GAGNPs in GLgels promote the formation of stable constructs without requiring a support bath or further chemical crosslinking (e.g., UV irradiation). In addition, the viscoelastic properties of GLgels prevent layer spreading or diffusion after extrusion.

To evaluate the structural stability of the constructs further, the printed vessels were immersed in cell culture media at 37 °C, and the dimensional changes were measured at different time points (7, 14, and 21 days) (Figure 5C). The results showed no significant alteration in the diameters and thicknesses of the cylinders, indicating the high structural stability of the printed constructs (Figure 5D).

3D Bioprinting

The physical and biochemical properties of bioinks directly affect cell fate. An ideal bioink should mix with cells while retaining viability during the printing process. Mixing and encapsulation of cells with viscous bioinks are often challenging and can negatively affect viability [64]. In contrast, the unagitated nature of GLgel formation facilitates the cell/bioink mixing process. In this process, the cells were first resuspended and mixed with GAGNPs suspension. Upon mixing with LA solution, a homogeneous gel was formed (Figure 5E). Here, we incorporated W-20–17 cells into 30GLgel and printed a lattice structure (Figure 5F).

F-actin staining was used to trace the cell spreading within the bioprinted constructs (Figures 5Fi–iii and S4). Uniform cell spreading and proliferation were observed in the 3D printed constructs at day 5 post printing (Figure 5Fiii). This result confirmed our hypothesis that the shear-thinning properties of GLgel can protect cells from stress and mechanical damage during the extrusion process [7]. Next, the metabolic activity of the cells encapsulated within the printed constructs was quantified using the PrestoBlue assay. The metabolic activity of the cells was increased from 1.1×10^4 at day 1 to 2.1×10^4 at day 7, indicating cell proliferation within the bioprinted 30GLgel (Figure 5G). Overall, these results confirmed that the GLgel effectively supports cell viability, spreading, and proliferation. Recent studies have also highlighted the cell supportive properties of shear-thinning biomaterials for tissue engineering applications [16, 19, 60]. However, the simplicity of the GLgel formation without any chemical modification, and ease of cell encapsulation makes it a promising candidate for biomanufacturing of 3D printed tissues.

In vivo biocompatibility and biodegradation of GLgel

30GLgel was selected for subcutaneous implantation study. All animals survived throughout the study without any malignancy, infection, or abscess at the injection sites. Tissues around the gel showed no necrosis or muscle degeneration, and mild adverse reactions such as inflammation and fibrosis (Figure 6). H&E staining showed that skin structure was intact, and no epidermal or dermal alterations or inflammatory infiltrates were detected, either 7 or 14 days after the injection. The surrounding tissue was spared from inflammation throughout the study period. Also, the H&E staining images revealed that biodegradation of 30GLgel allowed ingrowth of predominantly non-inflammatory cells and hydrogel replacement with the autologous tissue. These results confirmed that nanocomposite hydrogel could be effectively biodegraded *in vivo*.

4 Conclusion

In this study, we engineered a new class of shear-thinning biomaterials (GLgels) with tunable viscoelastic and mechanical properties for 3D bioprinting applications. The GLgel bioinks were formed through electrostatic interactions between synthetic smectic silicate nanosheets (LA) and glycosaminoglycan nanoparticles (GAGNPs). Shear-thinning and viscoelastic properties of the hydrogels with quick recovery responses were characterized. The GLgels can be straightforwardly printed to form complex construct with high shape retention without requiring additional crosslinking. Next, the ability of the engineered bioinks in supporting 3T3 and W-20–17 cells in both 2D and 3D culturing approaches was evaluated. *In vitro* studies indicated that the 3D bioprinted structures support cell adhesion, proliferation, and osteogenic differentiation of W-20–17 bone marrow stromal cells. F-actin staining also demonstrated cell spreading and attachment in the bioprinted constructs. High printability, shear-thinning properties, ease of and rapid crosslinking, high cytocompatibility, and bioactivity of the hydrogels endow their potential as a cell laden platform for developing functional 3D bioprinted scaffolds for regenerative medicine.

Supplementary Material

Refer to Web version on PubMed Central for supplementary material.

Acknowledgments

NA acknowledges the support from American Heart Association (AHA, 16SDG31280010), and National Institutes of Health (NIH) (R01EB023052; R01HL140618). AS wishes to thank the financial support of Iran National Science Foundation (INSF No. 95-S-48740) and Sharif University of Technology (Grant No. QA970816).

References:

[1]. Lutolf M, Hubbell J, Synthetic biomaterials as instructive extracellular microenvironments for morphogenesis in tissue engineering, Nature biotechnology 23(1) (2005) 47.

[2]. Cummins HZ, Liquid, glass, gel: The phases of colloidal Laponite, Journal of Non-Crystalline Solids 353(41–43) (2007) 3891–3905.

[3]. Eslahi N, Abdorahim M, Simchi A, Smart polymeric hydrogels for cartilage tissue engineering: A review on the chemistry and biological functions, Biomacromolecules 17(11) (2016) 3441–3463. [PubMed: 27775329]

[4]. Liu K, Zang S, Xue R, Yang J, Wang L, Huang J, Yan Y, Coordination Triggered Hierarchical Folate/Zinc Supramolecular Hydrogels Leading to Printable Biomaterials, ACS applied materials & interfaces 10 (2018) 4530–4539. [PubMed: 29336146]

[5]. Kim SH, Yeon YK, Lee JM, Chao JR, Lee YJ, Seo YB, Sultan MT, Lee OJ, Lee JS, Yoon S.-i., Precisely printable and biocompatible silk fibroin bioink for digital light processing 3D printing, Nature communications 9(1) (2018) 1620.

[6]. Liu K, Zang S, Xue R, Yang J, Wang L, Huang J, Yan Y, Coordination-triggered hierarchical folate/zinc supramolecular hydrogels leading to printable biomaterials, ACS applied materials & interfaces 10(5) (2018) 4530–4539. [PubMed: 29336146]

[7]. Chimene D, Peak CW, Gentry JL, Carrow JK, Cross LM, Mondragon E, Cardoso GB, Kaunas R, Gaharwar AK, Nanoengineered ionic–covalent entanglement (NICE) bioinks for 3D bioprinting, ACS applied materials & interfaces 10(12) (2018) 9957–9968. [PubMed: 29461795]

[8]. Zhu K, Shin SR, van Kempen T, Li YC, Ponraj V, Nasajpour A, Mandla S, Hu N, Liu X, Leijten J, Gold nanocomposite bioink for printing 3D cardiac constructs, Advanced functional materials 27(12) (2017) 1605352. [PubMed: 30319321]

[9]. Wang Q, Mynar JL, Yoshida M, Lee E, Lee M, Okuro K, Kinbara K, Aida T, Highwater-content mouldable hydrogels by mixing clay and a dendritic molecular binder, Nature 463(7279) (2010) 339. [PubMed: 20090750]

[10]. Hua J, Li Z, Xia W, Yang N, Gong J, Zhang J, Qiao C, Preparation and properties of EDC/NHS mediated crosslinking poly (gamma-glutamic acid)/epsilon-polylysine hydrogels, Materials Science and Engineering: C 61 (2016) 879–892. [PubMed: 26838920]

[11]. Annabi N, Zhang Y-N, Assmann A, Sani ES, Cheng G, Lassaletta AD, Vegh A, Dehghani B, Ruiz-Esparza GU, Wang X, Engineering a highly elastic human protein–based sealant for surgical applications, Science translational medicine 9(410) (2017) eaai7466. [PubMed: 28978753]

[12]. Mohammed Z, Hill S, Mitchell J, Covalent crosslinking in heated protein systems, Journal of food science 65(2) (2000) 221–226.

[13]. Holten-Andersen N, Harrington MJ, Birkedal H, Lee BP, Messersmith PB, Lee KYC, Waite JH, pH-induced metal-ligand cross-links inspired by mussel yield self-healing polymer networks with near-covalent elastic moduli, Proceedings of the National Academy of Sciences 108(7) (2011) 2651–2655.

[14]. Kim S-S, Lim S-H, Cho SW, Gwak S-J, Hong Y-S, Chang BC, Park MH, Song KW, Choi CY, Kim B-S, Tissue engineering of heart valves by recellularization of glutaraldehyde-fixed porcine valves using bone marrow-derived cells, Experimental & molecular medicine 38(3) (2006) 273. [PubMed: 16819286]

[15]. Umashankar P, Mohanan P, Kumari T, Glutaraldehyde treatment elicits toxic response compared to decellularization in bovine pericardium, Toxicology international 19(1) (2012) 51. [PubMed: 22736904]

[16]. Appel EA, Tibbitt MW, Webber MJ, Mattix BA, Veiseh O, Langer R, Self-assembled hydrogels utilizing polymer–nanoparticle interactions, Nature communications 6 (2015) 6295.

[17]. Ding X, Gao J, Awada H, Wang Y, Dual physical dynamic bond-based injectable and biodegradable hydrogel for tissue regeneration, Journal of Materials Chemistry B 4(6) (2016) 1175–1185. [PubMed: 32263010]

[18]. Peak CW, Stein J, Gold KA, Gaharwar AK, Nanoengineered colloidal inks for 3D bioprinting, Langmuir 34(3) (2017) 917–925. [PubMed: 28981287]

[19]. Thakur A, Jaiswal MK, Peak CW, Carrow JK, Gentry J, Dolatshahi-Pirouz A, Gaharwar AK, Injectable shear-thinning nanoengineered hydrogels for stem cell delivery, Nanoscale 8(24) (2016) 12362–12372. [PubMed: 27270567]

[20]. Avery RK, Albadawi H, Akbari M, Zhang YS, Duggan MJ, Sahani DV, Olsen BD, Khademhosseini A, Oklu R, An injectable shear-thinning biomaterial for endovascular embolization, Science translational medicine 8(365) (2016) 365ra156–365ra156.

[21]. Gaharwar AK, Kishore V, Rivera C, Bullock W, Wu CJ, Akkus O, Schmidt G, Physically Crosslinked Nanocomposites from Silicate-Crosslinked PEO: Mechanical Properties and

Osteogenic Differentiation of Human Mesenchymal Stem Cells, Macromolecular bioscience 12(6) (2012) 779–793. [PubMed: 22517665]

[22]. Chimene D, Lennox KK, Kaunas RR, Gaharwar AK, Advanced bioinks for 3D printing: a materials science perspective, Annals of biomedical engineering 44(6) (2016) 2090–2102. [PubMed: 27184494]

[23]. Malda J, Visser J, Melchels FP, Jüngst T, Hennink WE, Dhert WJ, Groll J, Hutmacher DW, 25th anniversary article: engineering hydrogels for biofabrication, Advanced materials 25(36) (2013) 5011–5028. [PubMed: 24038336]

[24]. Chimene D, Kaunas R, Gaharwar AK, Hydrogel bioink reinforcement for additive manufacturing: a focused review of emerging strategies, Advanced materials 32(1) (2020) 1902026.

[25]. Nojoomi A, Tamjid E, Simchi A, Bonakdar S, Stroeve P, Injectable polyethylene glycol-laponite composite hydrogels as articular cartilage scaffolds with superior mechanical and rheological properties, International Journal of Polymeric Materials and Polymeric Biomaterials 66(3) (2017) 105–114.

[26]. Muzzarelli RA, Greco F, Busilacchi A, Sollazzo V, Gigante A, Chitosan, hyaluronan and chondroitin sulfate in tissue engineering for cartilage regeneration: a review, Carbohydrate polymers 89(3) (2012) 723–739. [PubMed: 24750856]

[27]. Milev P, Friedlander DR, Sakurai T, Karthikeyan L, Flad M, Margolis RK, Grumet M, Margolis RU, Interactions of the chondroitin sulfate proteoglycan phosphacan, the extracellular domain of a receptor-type protein tyrosine phosphatase, with neurons, glia, and neural cell adhesion molecules, The Journal of Cell Biology 127(6) (1994) 1703–1715. [PubMed: 7528221]

[28]. Büttner M, Möller S, Keller M, Huster D, Schiller J, Schnabelrauch M, Dieter P, Hempel U, Over-sulfated chondroitin sulfate Derivatives induce osteogenic differentiation of hMSC independent of BMP-2 and TGF-β1 signalling, Journal of cellular physiology 228(2) (2013) 330–340. [PubMed: 22718137]

[29]. Xavier JR, Thakur T, Desai P, Jaiswal MK, Sears N, Cosgriff-Hernandez E, Kaunas R, Gaharwar AK, Bioactive nanoengineered hydrogels for bone tissue engineering: a growth-factor-free approach, ACS nano 9(3) (2015) 3109–3118. [PubMed: 25674809]

[30]. Zandi N, Mostafavi E, Shokrgozar MA, Tamjid E, Webster TJ, Annabi N, Simchi A, Biomimetic proteoglycan nanoparticles for growth factor immobilization and delivery, Biomaterials science 8(4) (2020) 1127–1136. [PubMed: 31389409]

[31]. Hinderer S, Seifert J, Votteler M, Shen N, Rheinlaender J, Schäffer TE, Schenke-Layland K, Engineering of a bio-functionalized hybrid off-the-shelf heart valve, Biomaterials 35(7) (2014) 2130–2139. [PubMed: 24333025]

[32]. Kerativitayanan P, Gaharwar AK, Elastomeric and mechanically stiff nanocomposites from poly (glycerol sebacate) and bioactive nanosilicates, Acta biomaterialia 26 (2015) 34–44. [PubMed: 26297886]

[33]. Sani ES, Lara RP, Aldawood Z, Bassir SH, Nguyen D, Kantarci A, Intini G, Annabi N, An antimicrobial dental light curable bioadhesive hydrogel for treatment of peri-implant diseases, Matter 1(4) (2019) 926–944. [PubMed: 31663080]

[34]. Noshadi I, Hong S, Sullivan KE, Sani ES, Portillo-Lara R, Tamayol A, Shin SR, Gao AE, Stoppel WL, Black III LD, In vitro and in vivo analysis of visible light crosslinkable gelatin methacryloyl (GelMA) hydrogels, Biomaterials science 5(10) (2017) 2093–2105. [PubMed: 28805830]

[35]. Soucy JR, Shirzaei Sani E, Portillo Lara R, Diaz D, Dias F, Weiss AS, Koppes AN, Koppes RA, Annabi N, Photocrosslinkable Gelatin/Tropoelastin Hydrogel Adhesives for Peripheral Nerve Repair, Tissue Engineering Part A 24 (2018) 1393–1405. [PubMed: 29580168]

[36]. Noshadi I, Walker BW, Portillo-Lara R, Sani ES, Gomes N, Aziziyan MR, Annabi N, Engineering biodegradable and biocompatible bio-ionic liquid conjugated hydrogels with tunable conductivity and mechanical properties, Scientific Reports 7(1) (2017) 4345. [PubMed: 28659629]

[37]. Ibrahim DM, Sani ES, Soliman AM, Zandi N, Mostafavi E, Youssef AM, Allam NK, Annabi N, Bioactive and elastic nanocomposites with antimicrobial properties for bone tissue regeneration, ACS Applied Bio Materials 3(5) (2020) 3313–3325.

[38]. Lorthioir C.d., Khalil M, Wintgens V.r., Amiel C, Segmental motions of poly (ethylene glycol) chains adsorbed on laponite platelets in clay-based hydrogels: a NMR investigation, Langmuir 28(20) (2012) 7859–7871. [PubMed: 22512344]

[39]. Nelson A, Cosgrove T, Dynamic light scattering studies of poly (ethylene oxide) adsorbed on laponite: Layer conformation and its effect on particle stability, Langmuir 20(24) (2004) 10382–10388. [PubMed: 15544363]

[40]. Nelson A, Cosgrove T, A small-angle neutron scattering study of adsorbed poly (ethylene oxide) on laponite, Langmuir 20(6) (2004) 2298–2304. [PubMed: 15835687]

[41]. Ding X, Gao J, Wang Z, Awada H, Wang Y, A shear-thinning hydrogel that extends in vivo bioactivity of FGF2, Biomaterials 111 (2016) 80–89. [PubMed: 27728816]

[42]. Das S, Zhou K, Ghosh D, Jha NN, Singh PK, Jacob RS, Bernard CC, Finkelstein DI, Forsythe JS, Maji SK, Implantable amyloid hydrogels for promoting stem cell differentiation to neurons, NPG Asia Materials 8(9) (2016) e304.

[43]. Rokita B, Rosiak JM, Ulanski P, Ultrasound-induced cross-linking and formation of macroscopic covalent hydrogels in aqueous polymer and monomer solutions, Macromolecules 42(9) (2009) 3269–3274.

[44]. Dong L, Agarwal AK, Beebe DJ, Jiang H, Adaptive liquid microlenses activated by stimuli-responsive hydrogels, Nature 442(7102) (2006) 551. [PubMed: 16885981]

[45]. Ladet S, David L, Domard A, Multi-membrane hydrogels, Nature 452(7183) (2008) 76.

[46]. Peppas NA, Hilt JZ, Khademhosseini A, Langer R, Hydrogels in biology and medicine: from molecular principles to bionanotechnology, Advanced materials 18(11) (2006) 1345–1360.

[47]. Shirzaei Sani E, Portillo-Lara R, Spencer A, Yu W, Geilich BM, Noshadi I, Webster TJ, Annabi N, Engineering adhesive and antimicrobial hyaluronic acid/elastin-like polypeptide hybrid hydrogels for tissue engineering applications, ACS Biomaterials Science & Engineering 4(7) (2018) 2528–2540. [PubMed: 33435116]

[48]. Dawson JI, Oreffo RO, Clay: new opportunities for tissue regeneration and biomaterial design, Advanced Materials 25(30) (2013) 4069–4086. [PubMed: 23722321]

[49]. Van Tomme SR, van Steenbergen MJ, De Smedt SC, van Nostrum CF, Hennink WE, Self-gelling hydrogels based on oppositely charged dextran microspheres, Biomaterials 26(14) (2005) 2129–2135. [PubMed: 15576188]

[50]. Wang H, Hansen MB, Löwik DW, van Hest JC, Li Y, Jansen JA, Leeuwenburgh SC, Oppositely charged gelatin nanospheres as building blocks for injectable and biodegradable gels, Advanced materials 23(12) (2011) H119–H124. [PubMed: 21394793]

[51]. Bohner M, Design of ceramic-based cements and putties for bone graft substitution, Eur Cell Mater 20(1) (2010) 3–10.

[52]. Haines-Butterick L, Rajagopal K, Branco M, Salick D, Rughani R, Pilarz M, Lamm MS, Pochan DJ, Schneider JP, Controlling hydrogelation kinetics by peptide design for three-dimensional encapsulation and injectable delivery of cells, Proceedings of the National Academy of Sciences 104(19) (2007) 7791–7796.

[53]. Sinclair A, O'Kelly MB, Bai T, Hung HC, Jain P, Jiang S, Self-Healing Zwitterionic Microgels as a Versatile Platform for Malleable Cell Constructs and Injectable Therapies, Advanced Materials 30(39) (2018) 1803087.

[54]. Cai L, Dewi RE, Heilshorn SC, Injectable hydrogels with in situ double network formation enhance retention of transplanted stem cells, Advanced functional materials 25(9) (2015) 1344–1351. [PubMed: 26273242]

[55]. Sani ES, Kheirkhah A, Rana D, Sun Z, Foulsham W, Sheikhi A, Khademhosseini A, Dana R, Annabi N, Sutureless repair of corneal injuries using naturally derived bioadhesive hydrogels, Science Advances 5 (2019) eaav1281. [PubMed: 30906864]

[56]. Schexnailder PJ, Gaharwar AK, Bartlett II RL, Seal BL, Schmidt G, Tuning Cell Adhesion by Incorporation of Charged Silicate Nanoparticles as Cross-Linkers to Polyethylene Oxide, Macromolecular bioscience 10(12) (2010) 1416–1423. [PubMed: 20602416]

[57]. Yesilyurt V, Webber MJ, Appel EA, Godwin C, Langer R, Anderson DG, Injectable self-healing glucose-responsive hydrogels with pH-regulated mechanical properties, Advanced materials 28(1) (2016) 86–91. [PubMed: 26540021]

[58]. Li L, Yan B, Yang J, Chen L, Zeng H, Novel mussel-inspired injectable self-healing hydrogel with anti-biofouling property, Advanced Materials 27(7) (2015) 1294–1299. [PubMed: 25581601]

[59]. Bai T, Sun F, Zhang L, Sinclair A, Liu S, Ella-Menye JR, Zheng Y, Jiang S, Restraint of the differentiation of mesenchymal stem cells by a nonfouling zwitterionic hydrogel, Angewandte Chemie 126(47) (2014) 12943–12948.

[60]. Mealy JE, Chung JJ, Jeong HH, Issadore D, Lee D, Atluri P, Burdick JA, Injectable granular hydrogels with multifunctional properties for biomedical applications, Advanced Materials 30(20) (2018) 1705912.

[61]. Shin M, Galarraga JH, Kwon MY, Lee H, Burdick JA, Gallol-derived ECM-mimetic adhesive bioinks exhibiting temporal shear-thinning and stabilization behavior, Acta biomaterialia 95 (2019) 165–175. [PubMed: 30366132]

[62]. Platt JL, Wrenshall LE, Johnson GB, Cascalho M, Heparan sulfate proteoglycan metabolism and the fate of grafted tissues, Immune Responses to Biosurfaces, Springer2015, pp. 123–140.

[63]. Ouyang L, Highley CB, Rodell CB, Sun W, Burdick JA, 3D printing of shear-thinning hyaluronic acid hydrogels with secondary cross-linking, ACS Biomaterials Science & Engineering 2(10) (2016) 1743–1751. [PubMed: 33440472]

[64]. Colosi C, Shin SR, Manoharan V, Massa S, Costantini M, Barbetta A, Dokmeci MR, Dentini M, Khademhosseini A, Microfluidic bioprinting of heterogeneous 3D tissue constructs using low-viscosity bioink, Advanced materials 28(4) (2016) 677–684. [PubMed: 26606883]

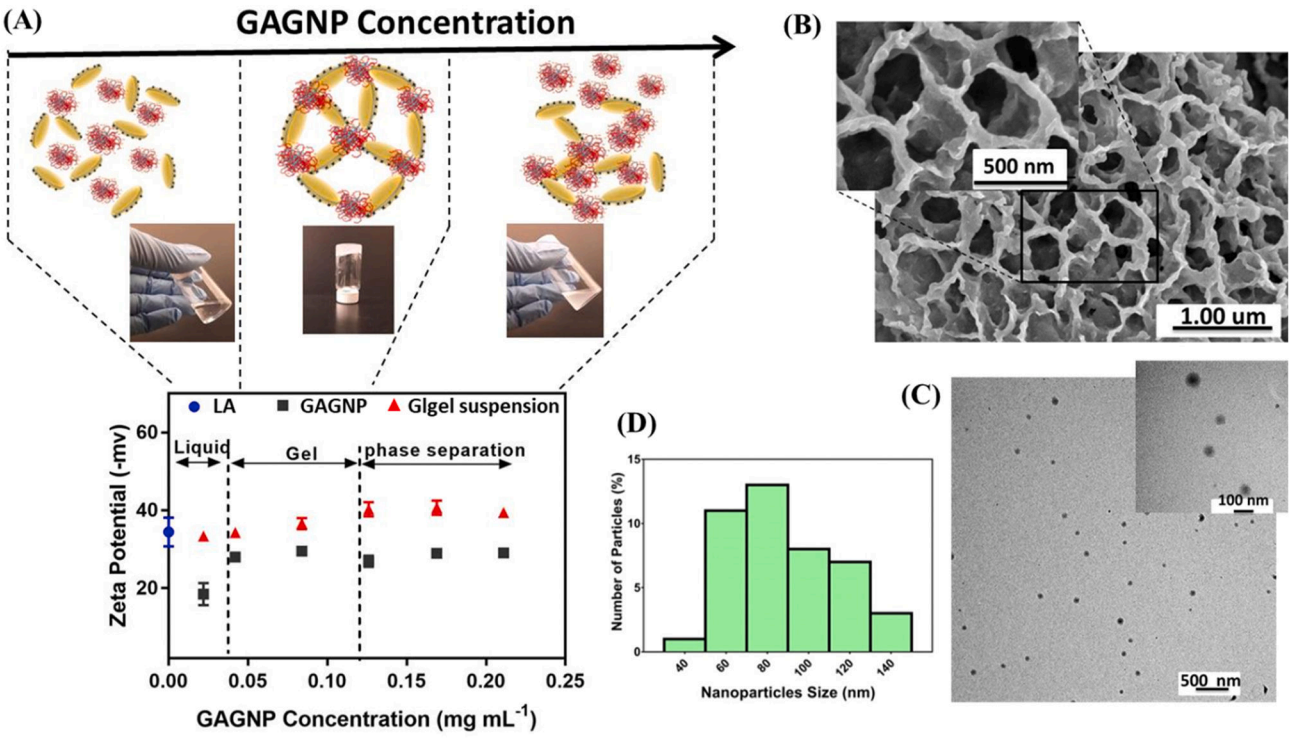

Figure 1.

Surface and topographical properties of glycosaminoglycan nanoparticle/laponite gel (GLgel). (A) Zeta potential measurements of laponite (LA), glycosaminoglycan nanoparticle (GAGNP) solution, and GLgel suspension (diluted GLgel) as a function of GAGNP concentration. For zeta potential measurement, GLgel suspension containing GAGNP (0.01 to 0.21 mg mL^{-1}), and LA (10 mg mL^{-1} LA) were used. (B) Representative scanning electron microscopy (SEM) images of 30GLgel showing the porous structure of the GLgel. (C) Representative transmission electron microscopy (TEM) image and (D) size distribution histogram of GAGNPs.

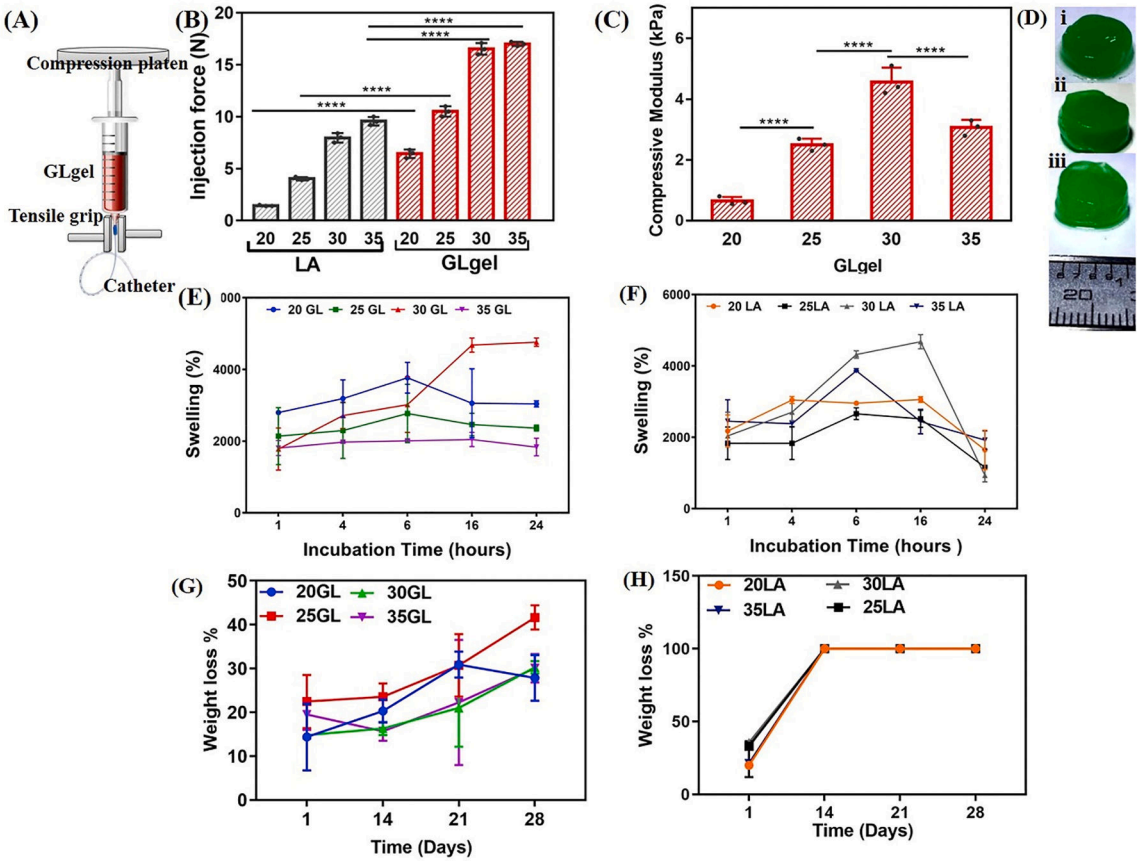

Figure 2.

Physical properties glycosaminoglycan nanoparticle/laponite (GLgel). (A) Schematic illustration of the injection force measurement system. (B) Quantitative analysis of the injection force for different laponite (LA) and GLgel compositions. (C) Compressive moduli of different GLgel compositions. Compression test on LA up to 35LA were not applicable (N/A). (D) Representative photographs of i) 20GL; ii) 30GL; and iii) 35GL, showing the shape-persistence and free-standing properties of the bioinks. (E,F) swelling ratios of GLgels and LA, respectively: up to 24 h incubation (37 °C) in Dulbecco's phosphate-buffered saline (DPBS). (G) and (H) *In vitro* degradation of GLgel and LA gels at different concentrations and incubated in DPBS for up to 28 days, respectively. Data show complete degradation of LA gels after 2 weeks of incubation. Data are presented as mean ± SD ($p < 0.05$: *, $p < 0.01$: **, $p < 0.001$: ***, and $p < 0.0001$: ****, $n \geq 3$).

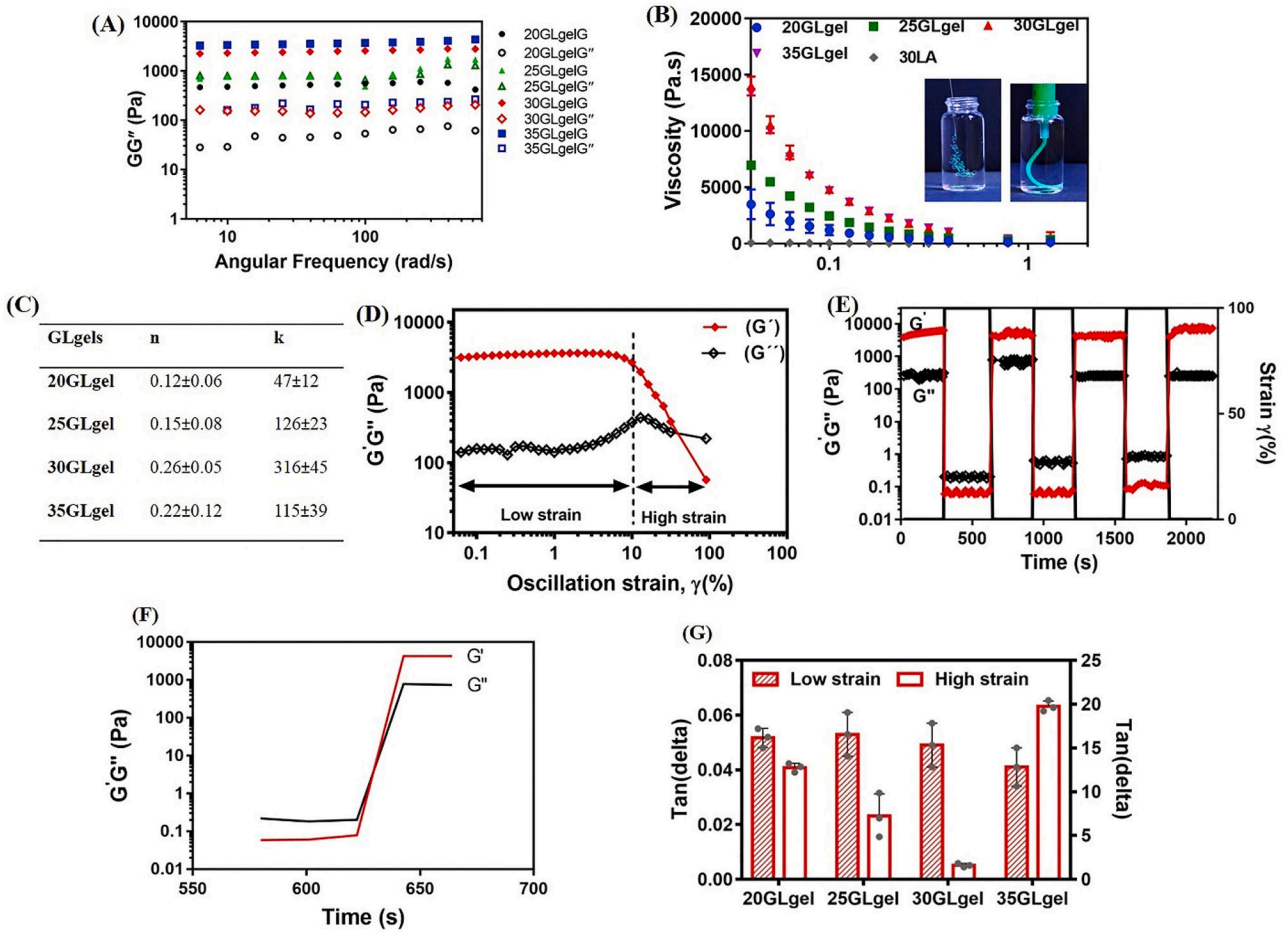

Figure 3.

Rheological characterization of glycosaminoglycan nanoparticle/laponite gel (GLgel). (A) Angular frequency sweep analysis of GLgels formed at different concentrations of GAG nanoparticle (GAGNP) and laponite (LA) (20, 30, 30, and 35GLgel). (B) Shear rate sweep of GLgels with different compositions with macroscopic images of the GLgel injection into Dulbecco's phosphate-buffered saline (DPBS). All GLgel compositions showed shear-thinning behavior in comparison to 30LA as a control, which showed Newtonian properties. (C) Summary of power-law parameters, showing non-Newtonian behavior of GLgels (D) Strain-dependent of G′G″ values for 30GLgel at 25 °C showing viscoelastic properties of the gel. (E) Step-strain measurements of 30GLgel over three cycles at 25 °C, demonstrating shear-recovery of the GLgels. (F) Overlaid zoom of the G′G″ values vs time (panel E) showing recovery of the GLgel after each cycle. (G) tan (delta) (G″/G′) of GLgels with different compositions at low and high strain. Data are presented as mean ± SD ($p < 0.05$: *, $p < 0.01$: **, $p < 0.001$: ***, and $p < 0.0001$: ****, $n \geq 3$).

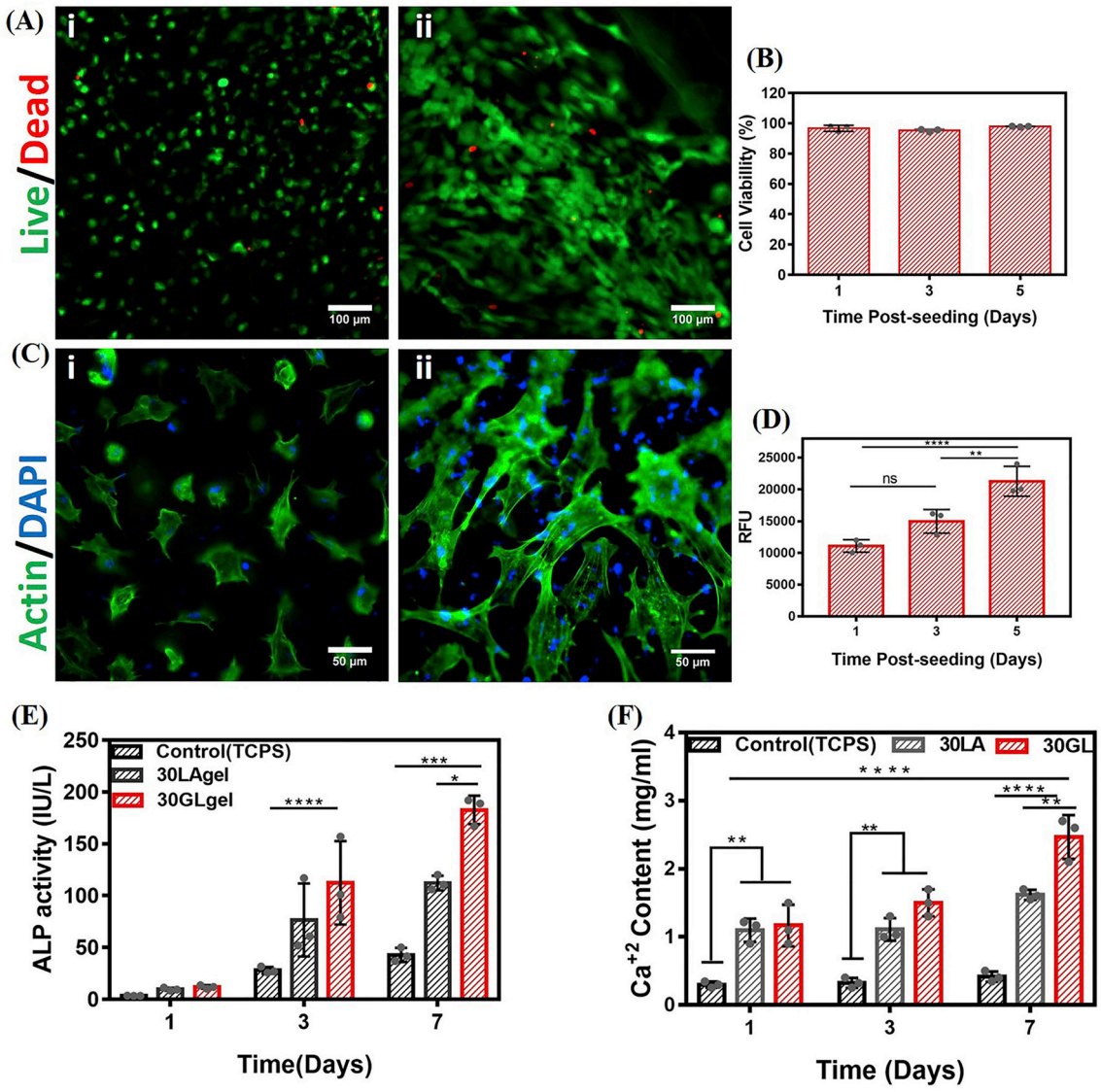

Figure 4.

In vitro cytocompatibility and osteogenic differentiation of W-20–17 cells encapsulated within Glycosaminoglycan nanoparticle/Laponite gel (GLgel). (A) Representative live/dead images of W-20–17 cells encapsulated within 30GLgel at days 1 (i) and 5 (ii). (B) Quantification of cell viability inside 30GLgel at days 1, 3, 5 post encapsulation. (C) Representative F-Actin fluorescent images of cells encapsulated in 30GLgel, at days 1 (i) and 5 (ii) post-encapsulation. (D) Metabolic activity of the 3D encapsulated cells within the 30GLgel on days 1, 3, and 5 post encapsulation. (E) Alkaline phosphatase activity of W-20–17 cells seeded on the surface of 30Glgel after 1, 3, and 7 days. (F) Quantification of calcium deposition W-20–17 cells seeded on the surface of 30Glgel after 1, 3, and 7 days. Data are presented as mean ± SD ($p < 0.05$: *, $p < 0.01$: **, $p < 0.001$: ***, and $p < 0.0001$: ****, $n \geq 3$).

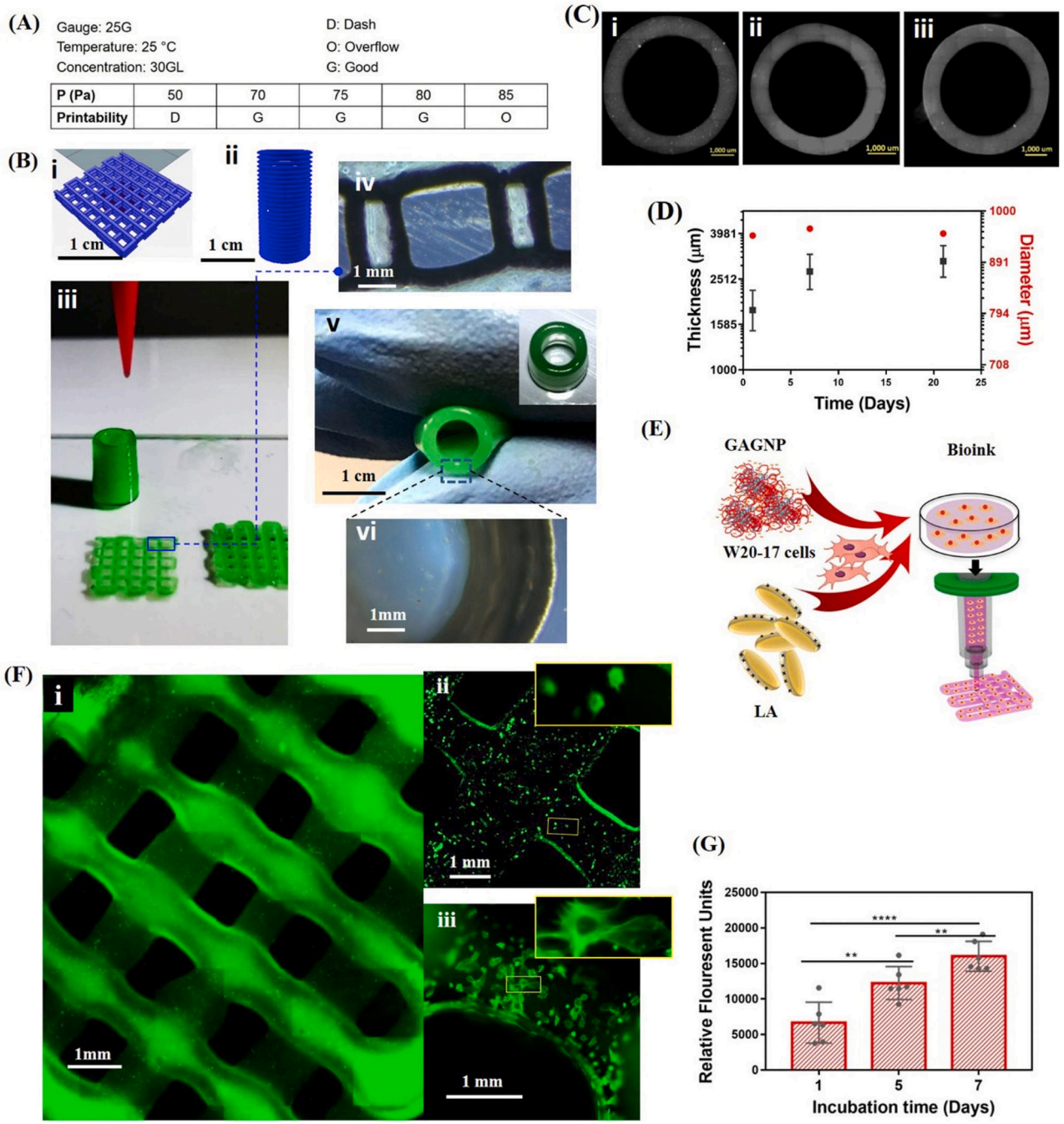

Figure 5.

3D bioprinting of Glycosaminoglycan nanoparticle/laponite (GLgel) to form cell-laden constructs. (A) Summary of the 3D printing parameters. (B) 3D printing of 30GLgel by extrusion printing: (Bi,ii) CAD models; (Biii) Fabrication based on CAD models; (Biv) Optical microscopy images of 3D-printed 30GLgel into rectangular shape; (Bv) Top view of a printed construct; (Bvi) Optical microscopy images of 3D-printed 30GLgel into cylindrical structure. (C) Representative phase-contrast images (top view) of tube structure after immersion in aqueous culture medium for (Ci) 1 week, (Cii) 2 weeks, and (Ciii) 3 weeks.

(D) Quantification of dimension stability of 3D-printed constructs in DPBS at different time points. (E) A schematic illustration of 3D bioprinting process, showing printing of cell-laden GLgel. (F) Representative fluorescence F-actin images of 3D bioprinted cell-laden 30GLgel after (Fi) 1 and (Fii) 5 days in cell culture. (G) Metabolic activity of W-20–17 cells within the bioprinted 30GLgel construct after 1, 5, and 7 days. Data are presented as mean ± SD ($p < 0.05$: *, $p < 0.01$: **, $p < 0.001$: ***, and $p < 0.0001$: ****, $n \geq 3$).

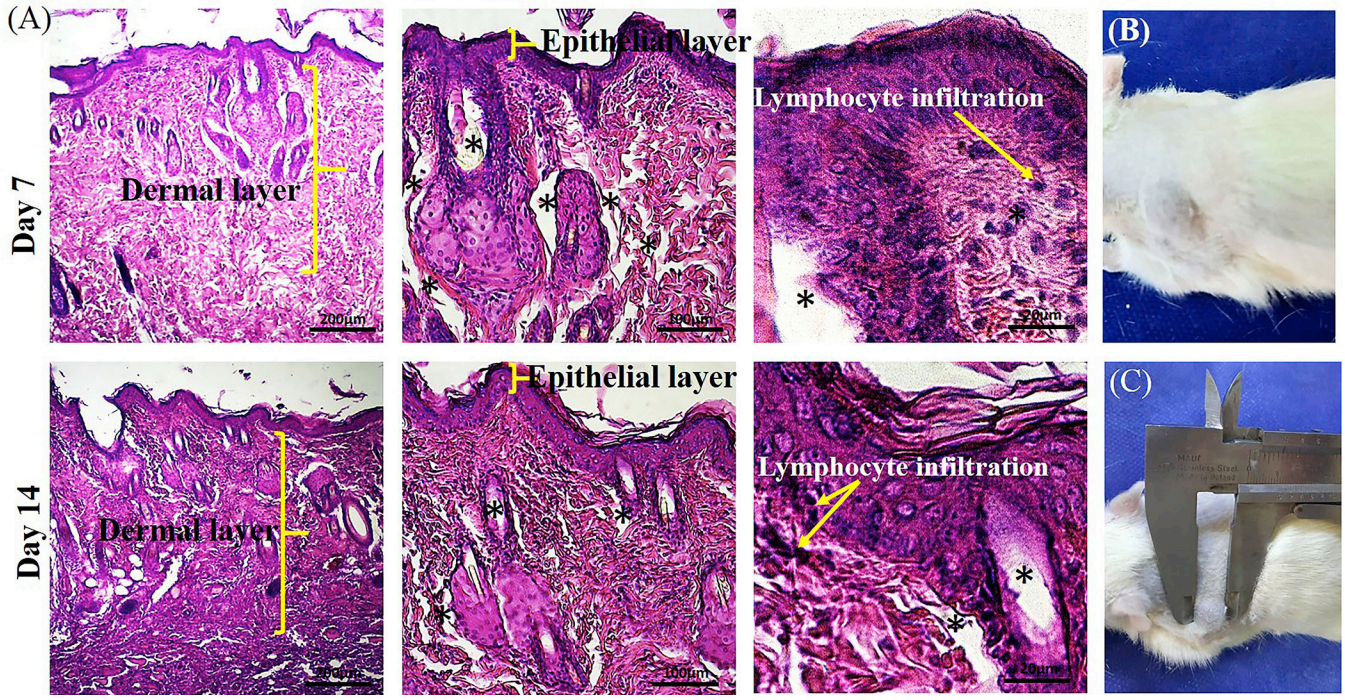

Figure 6.

In vivo biocompatibility and biodegradation of 30GLgel using a rat subcutaneous model. (A) Histopathological analysis of skin biopsies stained with H&E after 7 and 14 days. White asterisk: 30GLgel (B) Representative images of the implanted 30GLgel after 7 days, and (C) 14 days post-injection.

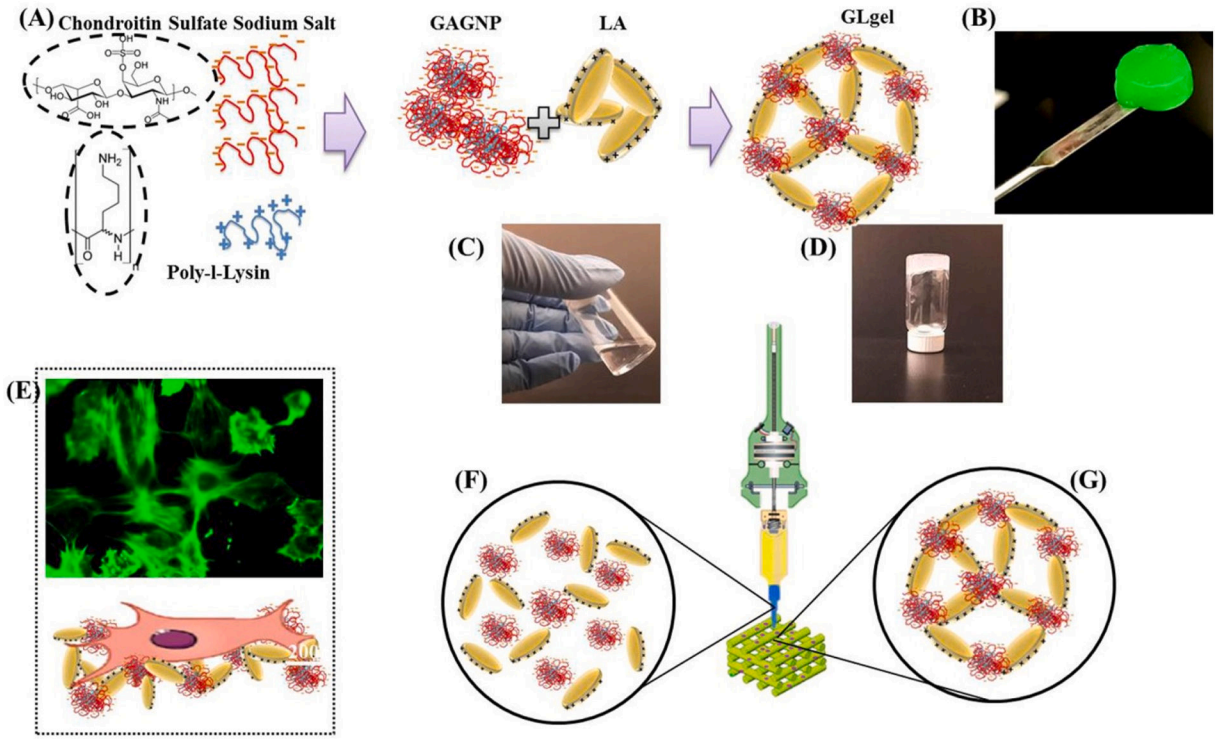

Scheme 1.

Synthesis and application of glycosaminoglycan nanoparticle/laponite gel (GLgel). (A) Schematic for the formation of glycosaminoglycan nanoparticles (GAGNPs), and the fabrication process for GLgel. The electrostatic interactions between chondroitin sulfate sodium salt (GAG) and poly-L-lysine (PLL) formed GAGNPs. The GLgel was then formed by mixing GAGNPs and LA. (B) Shape-persistent properties of GLgel. Representative images of (C) LA solution, and (D) GLgel. (E) Cell adhesion and spreading on GLgel. The structure of GLgel in (F) flow conditions (during extrusion), and (G) stress-relaxation status (after extrusion).

Table 1.

Samples Composition

Sample	20GLgel	25GLgel	30GLgel	35GLgel	20LA	25LA	30LA	35LA
LA conc. (mg ml^{-1})	20	25	30	35	20	25	30	35
GAGNP conc. (mg ml^{-1})	0.17	0.21	0.25	0.3	-	-	-	-